Complex and real unconventional Bose-Einstein condensations in high orbital bands

Zi Cai and Congjun Wu

Phys. Rev. A **84**, 033635 — Published 26 September 2011

DOI: 10.1103/PhysRevA.84.033635

Complex and real unconventional Bose-Einstein condensations in high orbital bands

Zi Cai and Congjun Wu
Department of Physics, University of California, San Diego, CA92093

We perform the theoretical study on the unconventional Bose-Einstein condensations (UBEC) in the high bands of optical lattices observed recently. These exotic states are characterized by complex-valued condensate wavefunctions with nodal points, or real-valued ones with nodal lines, thus are beyond the *"no-node"* theorem of the conventional BECs. A quantum phase transition is driven by the competition between the single particle band and interaction energies. The complex UBECs spontaneously break time-reversal symmetry, exhibiting a vortex-antivortex lattice structure.

PACS numbers: 03.75.Nt, 03.75.Lm, 05.30.Jp, 05.30.Rt

Quantum wavefunctions are generally complex-valued. However, the usual ground state wavefunctions of bosons are very restricted because they are positive-definite as stated in the *"no-node"* theorem [1]. This theorem applies under very general conditions: the kinetic energy is unfrustrated (e.g. the Laplacian-type); the single particle potential can be arbitrary; the two-body interaction depends only on coordinates. Mathematically, it is a direct consequence of the Perron-Frobenius theorem of matrix analysis [2]. This theorem implies that time-reversal (TR) symmetry cannot be spontaneously broken in various ground states of bosons, including superfluid, Mott-insulating, and supersolid states.

The "no-node" theorem, however, only applies to ground state, and hence not to meta-stable excited states of bosons. This opens up a possibility for *"unconventional"* states of bosons beyond the "no-node" theorem [3]. Similarly to unconventional superconductors, in unconventional Bose-Einstein condensations (UBEC), the condensate wavefunctions form non-trivial representations of the lattice symmetry groups. However, a major difference exists. Cooper pairs have the center of mass motion and the relative motion between two electrons of the pair. In unconventional superconductors, it is the relative motion that is non-trivial. The degree of freedom of the relative motion does not exist in the single boson BEC. In UBECs, the condensate wavefunctions are non-trivial.

Considerable efforts have been made to study unconventional states of bosons both experimentally and theoretically. Among the most exciting achievements are the realizations of the meta-stable excited states of bosons in high orbital bands [4–7], which leads to the opportunity to the study of the UBECs [8–15], and other exotic properties [16–21]. Below are some recent experimental results. Sebby-Strabley *et al.* succeeded in pumping a large fraction of bosons into the excited bands in a double-well lattice [4]. Mueller *et al.* observed the quasi-1D phase coherence pattern by exciting bosons into the p-orbital bands in the cubic lattice [5]. An important progress was made by the group of Hemmerich [6]: the UBECs in the sp-hybridized orbital bands were realized in a checkerboard-like lattice, which allows to establish the fully cross-dimensional coherence. More recently, UBECs in even higher orbital bands have been observed in the same group [7].

In this paper, we present the theoretical study on UBECs observed in the second, or, the first excited band, of the checkerboard optical lattice. This band is of a hybridized nature between the s-orbital of the shallower sites and the p-orbitals of the deeper sites. The lattice asymmetry favors a real-valued condensate wavefunction with nodal lines, while interactions favor a complex-valued one with nodal points. By solving the Gross-Pitaevskii (GP) equation for these meta-stable condensates, we find that tuning the lattice asymmetry drives the phase transition between these two types of UBECs in a good agreement with experimental observations.

We introduce the optical lattice employed in the experiment [6]. Each unit cell consists of two sites with different depths (denoted A and B below) as shown in Fig. 1 (a). (A similar lattice potential with different parameters has been plotted in Ref.[6]). The lattice is constructed by the interference pattern of phase coherent laser beams along $\pm x$ and $\pm y$-directions generated from a single laser through beam splitters and reflectors. The optical potential reads

$$\begin{aligned} V(x,y) &= -\frac{V_0}{4}|(\hat{z}\cos\alpha + \hat{y}\sin\alpha)e^{ik_l x} + \epsilon\hat{z}e^{-ik_l x} \\ &+ \eta e^{i\theta}\hat{z}(e^{ik_l y} + \epsilon e^{-ik_l y})|^2, \end{aligned} \tag{1}$$

where $\hat{y}$ and $\hat{z}$ are unit vectors describing light polarizations; k_l is the laser wavevector; $\epsilon < 1$ and $\eta < 1$ describe the imperfect reflection and transmission efficiencies; θ is the phase difference between beams along x and y-directions; α is used to tune the lattice asymmetry by rotating the light polarization out of the $\hat{z}$-direction.

The point group symmetry of this lattice is analyzed below. We start from the ideal case of $\epsilon = 1$ with $\alpha = 0^\circ$ and $\theta = 90^\circ$, at which A and B-sites are equivalent. At $\eta < 1$, the lattice has the reflection symmetries with respect to both the x and y-axes, thus the lattice is orthorhombic. Next we keep $\epsilon = 1$ and $\alpha = 0^\circ$ but set θ away from 90°. Then the unit cell includes both A and B-sites. The primitive lattice vectors are $a_0(\hat{e}_x \pm \hat{e}_y)$ where $a_0 = \pi/k_l$ as shown in Fig. 1 (b). The optical potential becomes $V = -\frac{V_0}{2}\big(\cos 2k_l x + \eta^2 \cos 2k_l y + 4\eta\cos\theta\cos k_l x \cos k_l y\big)$. θ

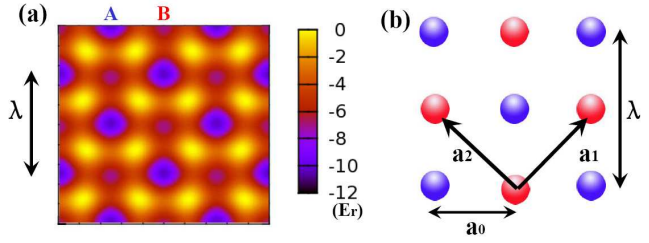

FIG. 1: (a) The optical lattice with the reflection symmetry with respect to the x-axis and the parameter values: $\eta = 0.95$, $\epsilon = 0.81$, $\theta = 95.4^\circ$, $\alpha = \alpha_0 = 36^\circ$ and $V_0 = 6.2E_r$. The A-sites have deeper potential depth than those of B-sites. (b) The basis vectors of the double-well lattice.

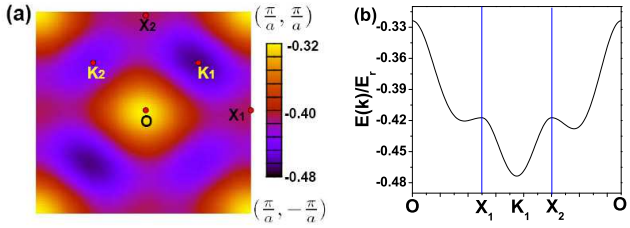

FIG. 2: (a) The energy spectra for the second band, the parameter values are the same as Fig.1 except $\alpha = 0^\circ$. (b) The spectra of (a) along the line from $(0, \frac{\pi}{a})$ to $(\frac{\pi}{a}, 0)$.

controls the potential difference between A and B sites. The point group symmetry remains orthorhombic. Now we move to the realistic case of $\epsilon < 1$. The unit cell remains double-well-shaped and the primitive lattice vectors are the same. However, the orthorhombic symmetry is broken and there is no point group symmetry for general values of parameters. This asymmetry can be partially compensated by setting $\alpha_0 = \cos^{-1}\epsilon$. We denote this configuration as "symmetric" and other ones with $\alpha \neq \alpha_0$ as "asymmetric" below. The symmetric lattice potential becomes $V = -\frac{V_0}{2}\epsilon\big(\epsilon\cos 2k_l x + \eta^2\cos 2k_l y\big) - V_0\eta\epsilon\cos k_l x\big[\cos(k_l y+\theta)+\epsilon^2\cos(k_l y-\theta)\big]$, which has the reflection symmetry with respect to the x-axis but not to the y-axis.

Next we calculate the band structures. The reciprocal lattice vectors are defined as $\vec{G}_{m,n} = m\vec{b}_1 + n\vec{b}_2$ with $\vec{b}_{1,2} = (\pm\frac{\pi}{a}, \frac{\pi}{a})$. The single particle Hamiltonian reads as $H_0 = -\hbar^2\vec{\nabla}^2/(2M) + V(r)$ where M is the boson mass. Using the plane wave basis, the diagonal matrix elements are $\langle\vec{k}+\vec{G}_{mn}|H_0|\vec{k}+\vec{G}_{mn}\rangle = E_r\{[ak_x/\pi + (m-n)]^2 + [ak_y/\pi + (m+n)]^2\}$, where $E_r = \hbar^2\pi^2/(2Ma^2)$ is the recoil energy. The off-diagonal matrix elements read

$$\begin{aligned}
\langle\vec{k}|H_0|\vec{k}+\vec{G}_{\pm1,0}\rangle &= -\frac{V_0}{4}\eta\epsilon(\cos\alpha e^{\mp i\theta} + e^{\pm i\theta}),\\
\langle\vec{k}|H_0|\vec{k}+\vec{G}_{0,\pm1}\rangle &= -\frac{V_0}{4}\eta(\cos\alpha e^{\pm i\theta} + \epsilon^2 e^{\mp i\theta}),\\
\langle\vec{k}|H_0|\vec{k}+\vec{G}_{\pm1,\mp1}\rangle &= -\frac{V_0}{4}\epsilon\cos\alpha,\\
\langle\vec{k}|H_0|\vec{k}+\vec{G}_{\pm1,\pm1}\rangle &= -\frac{V_0}{4}\epsilon\eta^2\cos\alpha. \qquad (2)
\end{aligned}$$

We focus on the second band into which bosons are pumped [6]. There are four points in the Brillouin zone (BZ), *i.e.*, $O = (0,0)$, $K_{1,2} = (\pm\frac{\pi}{2a_0}, \frac{\pi}{2a_0})$, and $M = (\frac{\pi}{a_0}, \frac{\pi}{a_0})$, at which the Bloch wavefunctions are TR invariant, and thus real-valued. The band spectra are symmetric with respect to these points, which means that they are local energy extrema or saddle points. For the symmetric lattice with $\alpha = \alpha_0$, the second band has doubly degenerate energy minima of the states $\psi_{K_{1,2}}$ located at $K_{1,2}$, respectively. For the asymmetric case, the degeneracy between ψ_{K_1} and ψ_{K_2} are lifted. For $\alpha < (>)\alpha_0$, $K_1(K_2)$ become the band minimum, respectively. The energy spectra of $\alpha = 0$ is shown in Fig. 2 (a) and (b) (A similar energy spectrum with different parameters has been plotted in Ref.[6]).

The real space distributions of $\psi_{K_{1,2}}$ are also calculated. Their nodal lines pass the centers of the deeper sites of A. Thus the orbital component on the A-sites is of the p-type and that on the shallower sites of B is of the s-type. In fact, the p-orbital configurations of $\psi_{K_{1,2}}(\vec{r})$ in the A-sites are actually not exactly along the directions of $\hat{e}_x \pm \hat{e}_y$ because of the lack of the tetragonal symmetry. This point is mostly clear in the case of strong potentials so that we can define local orbitals on each site. Even for the symmetric lattice, the p_x and p_y-orbitals on the A-sites can be defined according to their parities under the reflection with respect to the x-axis. However, they are non-degenerate. The orbital components of $\psi_{K_{1,2}}(\vec{r})$ are nearly the same on A-sites, *i.e.*, mostly the lower energy p-orbital slightly hybridized with the higher one. The orthogonality of these two states comes from their different lattice momenta.

Interactions determine the configurations of UBECs in the presence of degenerate band minima. Any linear superposition among them gives rise to the condensate wavefunctions with the same kinetic energy. However, interactions break this degeneracy. Previous studies on p-orbital BECs based on tight-binding models predicted linear superpositions between two Bloch wavefunctions at degenerate band minima with a phase difference $\pm\frac{\pi}{2}$. Such a condensate breaks TR symmetry spontaneously [3, 8]. Bosons on p-orbital sites aggregate into the $p_x \pm ip_y$ states to reduce their repulsive interaction energy. This is a result of the second Hund's rule: complex p-orbitals are spatially more extended than the real orbitals, and thus bosons have more room to avoid each other.

The optical potential in the current experiment is shallow, thus the system is in the weak correlation regime [6]. Instead of the tight-binding model, we use the GP equation. Because of the absence of the lattice potential along the z-axis, we neglect the z-dependence of the condensate wavefunction. We only consider its distribution $\Psi(\vec{r})$ in the xy-plane. It is normalized as $\frac{1}{\Omega}\int' d^2r|\Psi(\vec{r})|^2 = 1$ where $\int' d^2\vec{r}$ integrates over one unit cell with the area

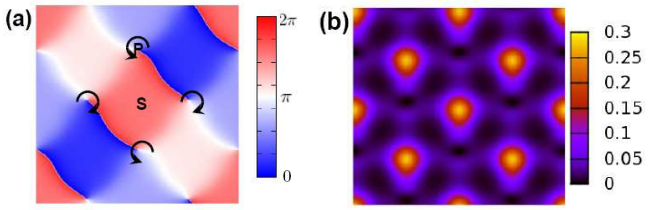

FIG. 3: The distributions of (a) the phase and (b) density patterns of the complex UBEC. The parameter values are the same as in Fig.1 except $g\rho_0 = 0.6E_r$ and $\alpha = 36°$. The vortex and anti-vortex cores are located in the centers of A-sites.

of $\Omega = 2a_0^2$. The GP equation reads

$$\Big\{ -\frac{\hbar^2\vec{\nabla}^2}{2M} + V(\vec{r}) + g\rho_0|\Psi(\vec{r})|^2 \Big\}\Psi(\vec{r}) = E\Psi(\vec{r}), \quad (3)$$

where $\rho_0 = N_0/V$ is the average 3D density with N_0 the total boson number in the condensate and V is the 3D volume of the system; g is the s-wave scattering interaction parameter. In the calculations below, various values of interaction parameters $g\rho_0$ are used from 0 up to E_r, which is of the same order of magnitude with the bandwidth. For this intermediate interaction, the GP equation is known to provide a good description of the system.

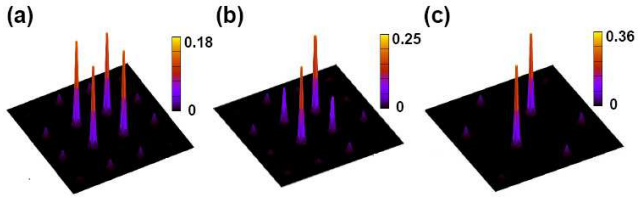

FIG. 4: Density distribution in the time-of-flight spectrum for (a)complex condensate in the symmetric case ($\alpha = 36.0°$) (b)complex condensate in the asymmetric case ($\alpha = 35.5°$). (c)real condensate ($\alpha = 34.5°$). Other parameters values are the same as Fig.1 except α.

Although Eq. 3 looks the same as the usual GP equation, the marked difference is that $\Psi(\vec{r})$ is not the ground state condensate but the meta-stable one belonging to the second band. The non-linearity of the GP equation allows mixing between different Bloch wave states. Let us start from the symmetric lattice with $\alpha = \alpha_0$. Eq. 3 is solved self-consistently as follows. We define the renormalized potential as $V_{eff}(\vec{r}) = V(\vec{r}) + g\rho_0|\Psi(\vec{r})|^2$, and solve the corresponding renormalized band structure. Then the condensate wavefunction is optimized to minimize the total energy, which in turn determines V_{eff}. The renormalized band structure is similar to the free one, which still has two degenerate band minima at $K_{1,2}$. We define the condensate wavefunction as

$$\Psi(\vec{r}) = \cos\delta\ \psi_{K_1}(\vec{r}) + e^{i\phi}\sin\delta\ \psi_{K_2}(\vec{r}). \quad (4)$$

The total energy reaches minimal at $\delta = \frac{\pi}{4}$ and $\phi = \pm\frac{\pi}{2}$. Notice that the point $\phi = 0$ also represents a metastable stationary state which exhibits nontrivial dynamical instability[22–24], which is beyond the scope of our paper. These complex condensate wavefunctions only have nodal points, while the real ones $\psi_{K_{1,2}}$ have nodal lines. The complex ones are spatially more uniform, and thus are favored by interactions. We plot the phase and density patterns of this condensate in Fig. 3, which exhibit a vortex-antivortex lattice structure. The vortex and anti-vortex cores are located alternatively at centers of A-sites, at which the antiferromagnetic order of orbital angular momentum develops. For every closest four B-sites, their phases wind around the central A-site following the same vorticity. This is similar to the case of the tight-binding models [3, 8]. The Bragg peaks in the time of flight (TOF) spectra are located at $(m+\frac{1}{2})\vec{b}_1 + n\vec{b}_2$ and $m\vec{b}_1 + (n+\frac{1}{2})\vec{b}_2$ as observed in the experiment [6]. In particular, the four peaks of $\pm\frac{1}{2}\vec{b}_{1,2} = (\pm\frac{\pi}{2a_0}, \pm\frac{\pi}{2a_0})$ are strongest with equal intensities, as shown in Fig.4 (a).

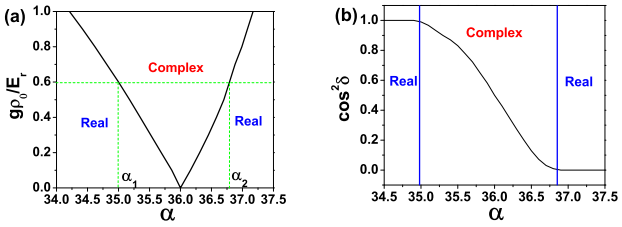

FIG. 5: (a)The phase diagram as a function of α and the interaction strength $g\rho_0$. Other parameters values are the same as Fig.2. (b) The condensate fractions of ψ_{K_1} in the complex UBEC $\Psi = \cos\delta\ \psi_{K_1} \pm i\sin\delta\ \psi_{K_2}$, the parameter values are the same as Fig.1 except α and $g\rho_0 = 0.6E_r$.

Now we move to the asymmetric lattice whose free band structure minimum is non-degenerate. The complex condensates are favored by interactions, and thus should be stable at asymmetries weak enough. Certainly, at large asymmetries, the real condensate wins due to the gain of band energy. This picture is explicitly confirmed by the phase diagram calculated by GP equation. As shown in Fig. 5 (a), for a given value of the interaction strength $g\rho_0$, the complex condensate in the form of Eq. 4 is stable in a finite parameter range from α_1 to α_2, beyond this regime the condensate changes to the real one, and the TOF spectra of such a real condensate only contain peaks of $(m+\frac{1}{2})\vec{b}_1$ or $(m+\frac{1}{2})\vec{b}_2$, as shown in Fig.4 (c)

In the complex condensate, the relative phase ϕ between $\psi_{K_{1,2}}$ is always $\pm\frac{\pi}{2}$, *i.e.*, Ψ and Ψ^* are degenerate as TR partners; δ is asymmetry dependent. The spatial asymmetry of $|\Psi(\vec{r})|^2$ depends on that of the bare potential V. However, V_{eff}, a combination of V and $|\Psi|^2$, becomes symmetric. Without loss of generality, $\Psi(\vec{r})$ is expanded in terms of two orthonormal real wavefunctions $\psi_{1,2}(\vec{r})$ in the same way as in Eq. 4 by replacing $\psi_{K_{1,2}}$ with $\psi_{1,2}$. Apparently, both $\Psi(\vec{r})$ and $\Psi^*(\vec{r})$ satisfy Eq.

3, and yield the same V_{eff}. The corresponding renormalized single particle Hamiltonian, $-\hbar^2\nabla^2/(2M) + V_{eff}$, has degenerate band minima $\psi_{1,2}$. However, please note that the superposition principle does not apply to the non-linear GP equation: $\psi_{1,2}$ are *not* solutions to Eq. 3. $|\Psi(\vec{r})|^2$ is also asymmetric depending on the asymmetry of the bare potential V. The TOF spectra still exhibit four dominant peaks at $\pm(\frac{\pi}{2a_0}, \frac{\pi}{2a_0})$ and $\pm(-\frac{\pi}{2a_0}, \frac{\pi}{2a_0})$, as shown in Fig.4 (b). The relative intensities of these two pairs of peaks depend on the lattice asymmetry, which can be reflected by the condensation fractions ψ_{K_1} in the complex condensate, as plotted in Fig. 5 (b). An observation of the asymmetric peaks at $\pm\frac{1}{2}\vec{b}_{1,2}$ at $\alpha_1 < \alpha < \alpha_2$ would provide a supporting evidence for the complex condensates. The TOF spectra lack phase information, thus the observation of the symmetric peaks $\pm\frac{1}{2}\vec{b}_{1,2}$ at α_0 [6] could be interpreted as the phase separation of real condensates of $\psi_{K_{1,2}}$, or an incoherent mixing between them. However, in these scenarios, the lattice asymmetry lifts the degeneracy and only leads to one pair of peaks. Even two condensates could coexist forming domains, the condensate fraction of ψ_{K_1} in the complex condensate should not follow that plotted in Fig. 5(b).

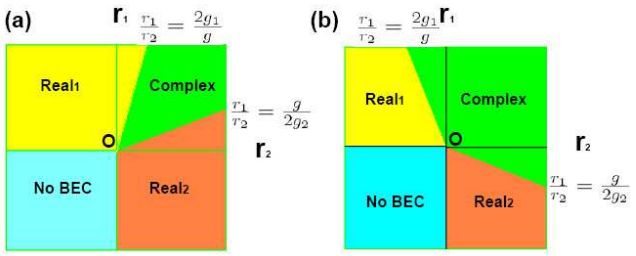

FIG. 6: Phase diagram as a function of r_1, r_2 predicted by Eq.6 for (a) $g > 0$; (b) $g < 0$.

For a better understanding of phase transitions between real and complex UBECs, we construct a Ginzburg-Landau (GL) free energy as:

$$\begin{aligned} F &= -r_1|\Psi_{K_1}|^2 - r_2|\Psi_{K_2}|^2 + g_1|\Psi_{K_1}|^4 + g_2|\Psi_{K_2}|^4 \\ &+ g_3|\Psi_{K_1}|^2|\Psi_{K_2}|^2 + g_4(\Psi^*_{K_1}\Psi^*_{K_1}\Psi_{K_2}\Psi_{K_2} + h.c), \quad (5) \end{aligned}$$

where $\Psi_{K_{1,2}} = \psi_{K_{1,2}}e^{i\theta_{1,2}}$ describe the condensate order parameters at $K_{1,2}$; $\theta_{1,2}$ are the phases of the condensates of $\Psi_{K_{1,2}}$ and $\psi_{1,2}$ are real as explained before. Although $\Psi_{K_{1,2}}$ do not couple at the quadratic level due to the requirement of translational symmetry, they do couple at the quartic level as in the g_4 term because $\pm 2(\vec{K}_1 - \vec{K}_2)$ equals reciprocal lattice vectors. g_4 is positive for repulsive interactions which favors the relative phase difference $\theta_1 - \theta_2 = \pm\frac{\pi}{2}$, thus the free energy in Eq.(5) can be reduced to:

$$F = -r_1\psi^2_{K_1} - r_2\psi^2_{K_2} + g_1\psi^4_{K_1} + g_2\psi^4_{K_2} + g\psi^2_{K_1}\psi^2_{K_2}, \quad (6)$$

in which $g = g_3 - 2g_4$. We define $G = 4g_1g_2 - g^2$ and $g_1, g_2, G > 0$ as required by the thermodynamic stability condition. In the superfluid regime, the complex UBEC is characterized by the non-zero values of both $\Psi_{K_{1,2}}$, while the real BECs correspond to one of these values being zero. Without loss of generality, we fix g_1, g_2, g and plot the phase diagram of the superfluid regime as a function of r_1, r_2. As shown in Fig.6, for $g > 0$, the complex BECs occur when $\frac{g}{2g_2} < \frac{r_1}{r_2} < \frac{2g_1}{g}$, where both r_1, r_2 are positive. It is interesting to notice that for $g < 0$, the complex BEC can exist even one channel is off-critical ($r_1 < 0$ or $r_2 < 0$), which means that in this case, the complex BEC is purely induced by interaction. A similar phase diagram has been proposed in a different context about p-wave resonant Bose gas[25, 26].

As interaction increases, and the system is brought into the Mott insulating regime. Nevertheless, at least in the weakly insulating regime, the suppress of the superfluidity ordering is due to phase fluctuations, and the magnitudes of $|\Psi_{K_{1,2}}|$ remain nonzero. Though θ_1 and θ_2 are disordered such that $\langle\Psi_{K_{1,2}}\rangle = 0$, their relative phase $\theta_1 - \theta_2 = \pm\frac{\pi}{2}$. This indicates a TR breaking order with a bilinear form of $\Psi_{K_{1,2}}$ as $L = i\langle\Psi^*_{K_1}\Psi_{K_2} - \Psi^*_{K_2}\Psi_{K_1}\rangle$ in the Mott insulating state. Its physical meaning here remains the staggered circulating currents, i.e., this exotic Mott insulating states preserve the antiferromagnetic OAM order of the complex BECs but not the global phase coherence.

In summary, we have studied the UBECs observed in high orbitals bands in Ref.[6]. The unconventional condensate wavefunctions can be real and TR invariant with nodal lines, or complex breaking TR symmetry with nodal points. In both cases, translational symmetry is broken due to the nonzero condensation wavevectors, thus these UBECs can be considered as unconventional supersolid states. The interplay between lattice asymmetry and interactions drives the transition between them.

We are grateful to A. Hemmerich for carefully reading our manuscript and insightful discussions. We also thank A. Hemmerich, C. Morais Smith and O. Tieleman for pointing out a mistake in the earlier version of the draft about the order of the phase transition. Z.C. and C.W. are supported by NSF DMR-1105945 , and the AFOSR-YIP program.

[1] R. P. Feynman, *Statistical Mechanics, A Set of Lectures* (Addison-Wesley Publishing Company, 1972).
[2] R. B. Bapat and T. Raghavan, *Non-negative matrices and applications* (Cambridge Univ. Press, 1997).
[3] C. Wu, Mod. Phys. Lett. B **23**, 1 (2009), 0901.1415.
[4] J. Sebby-Strabley, M. Anderlini, P. S. Jessen, and J. V.

Porto, Phys. Rev. A **73**, 033605 (2006).
[5] T. Müller, S. Fölling, A. Widera, and I. Bloch, Phys. Rev. Lett. **99**, 200405 (2007).
[6] G. Wirth, M. Ölschläger, and A. Hemmerich, Nature Physics **7**, 147 (2011).
[7] M. Ölschläger, G. Wirth, and A. Hemmerich, Phys. Rev. Lett. **106**, 015302 (2011).
[8] W. V. Liu and C. Wu, Phys. Rev. A **74**, 13607 (2006).
[9] A. Isacsson and S. M. Girvin, Phys. Rev. A **72**, 053604 (2005).
[10] O. E. Alon, A. I. Streltsov, and L. S. Cederbaum, Phys. Rev. Lett. **95**, 030405 (2005).
[11] C. Wu, W. V. Liu, J. E. Moore, and S. Das Sarma, Phys. Rev. Lett. **97**, 190406 (2006).
[12] V. M. Stojanović, C. Wu, W. V. Liu, and S. Das Sarma, Phys. Rev. Lett. **101**, 125301 (2008).
[13] A. B. Kuklov, Phys. Rev. Lett. **97**, 110405 (2006).
[14] J.-P. Martikainen, Phys. Rev. A **83**, 013610 (2011).
[15] M. Lewenstein and W. V. Liu, Nature Physics **7**, 101 (2011).
[16] C. Wu, D. Bergman, L. Balents, and S. D. Sarma, Phys. Rev. Lett. **99**, 70401 (2007).
[17] V. M. Scarola and S. Das Sarma, Phys. Rev. Lett. **95**, 033003 (2005).
[18] C. Xu and M. P. A. Fisher, Phys. Rev. B **75**, 104428 (2007).
[19] J. H. Challis, S. M. Girvin, and L. I. Glazman, Phys. Rev. A **79**, 043609 (2009).
[20] X. Li, E. Zhao, and W. V. Liu, Phys. Rev. A **83**, 063626 (2011).
[21] Q. Zhou, J. V. Porto, and S. Das Sarma, Phys. Rev. B **83**, 195106 (2011).
[22] V. S. Shchesnovich and V. V. Konotop, Phys. Rev. Lett. **102**, 055702 (2009).
[23] V. S. Shchesnovich, Phys. Rev. A **80**, 031601 (2009).
[24] V. S. Shchesnovich and V. V. Konotop, Phys. Rev. A **75**, 063628 (2007).
[25] S. Choi and L. Radzihovsky, ArXiv e-prints (2011), 1106.5765.
[26] L. Radzihovsky and S. Choi, Phys. Rev. Lett. **103**, 095302 (2009).